AIAA JOURNAL
Vol. 43, No. 7, July 2005

Control of Flow Around Square Cylinders at Incidence by Using a Rod

Mustafa Sarioglu,* Yahya Erkan Akansu,† and Tahir Yavuz‡
Karadeniz Technical University, 61080 Trabzon, Turkey

Aerodynamic characteristics of a square cylinder at incidence were investigated experimentally in the wake of a small rod at a Reynolds number of 3.4×10^4. The dimensionless gap L/D was varied from 1.71 to 8.00. Depending on the spacing L/D, two flow patterns with and without vortex shedding from the rod were observed. Pressure measurements on the rod and square cylinder and hot-film measurements in the wake of the cylinder were carried out. The combined influences of the rod and angle of incidence on the pressure distributions and vortex-shedding phenomenon were investigated. Without the rod, as the incidence increases from 0 deg, the reattachment on the lower side surface of the square cylinder occurs at the vicinity of 13 deg, and this corresponds to a jump in the Strouhal number. However, when the rod was set upstream of the square cylinder, the reattachment occurs at smaller angles of incidence depending on L/D. At zero angle of incidence, the minimum value of drag on the square cylinder is obtained for $L/D = 2.0$ and produces a drag that is 30% that of the square cylinder without rod. For $L/D = 1.71$, with increasing the angle of incidence C_D values approximate to those of the square cylinder without rod. In the case of $L/D \geq 2.7$, there is a considerable decrease in C_D in the region $\theta \leq 10$ deg; however, the effect of the rod on C_D decreases beyond $\theta = 10$ deg.

Nomenclature

C_D	=	drag coefficient of square cylinder based on D as the reference length
C_{DR}	=	drag coefficient of rod
C_{DT}	=	total drag coefficient, $= C_D + C_{\mathrm{DR}}(d/D)$
C_L	=	lift coefficient of square cylinder based on D as the reference length
C_p	=	pressure coefficient, $= (P - P_{\mathrm{st}})/\frac{1}{2}\rho U^2$
D	=	length of side of square cylinder
D'	=	projected cross-stream dimension of the square cylinder in incidence
d	=	diameter of rod
f	=	vortex-shedding frequency
L	=	distance between the axes of square cylinder and rod
P	=	surface pressure
P_{st}	=	static pressure in the test section
Re	=	Reynolds number based on D, UD/ν
Sr	=	Strouhal number based on D
Sr'	=	Strouhal number based on D'
U	=	freestream velocity
x, y	=	streamwise and lateral coordinates
α	=	circumferential angle measured from the front stagnation point of the rod
θ	=	angle of incidence
ν	=	kinematic viscosity of fluid
ρ	=	density of air

I. Introduction

CIRCULAR and square cylinders are typical shapes used in numerous construction and equipment. Many numerical and experimental studies have been carried out to understand the characteristics of the flow around these bluff bodies. Besides, in many engineering applications objects often appear in the wake of another obstacle. It is well known that two bodies that are closely placed in a tandem arrangement in a flow show strong aerodynamic interference with each other because of the effects of the wake generated by the upstream body.[1] For this reason, pressure distributions and vortex-shedding patterns of bodies in arrangement are entirely different from those of the individual bodies.

Two circular cylinders in tandem arrangement have been studied in many works for the various gaps between two cylinders and flow conditions such as Reynolds number and turbulent levels. Extensive reviews were given by Zdravkovich,[2] who also discussed the cases of side-by-side and staggered arrangements. Arie et al.[3] studied pressure fluctuations on the surface of two circular cylinders. The other investigations of this configuration were conducted by Okajima,[4] Igarashi,[5] Shiraishi et al.,[1] Gu,[6] and Alam et al.[7]

Two circular cylinders of different diameters along with the use of a small rod upstream of a bluff body for drag reduction have been studied by many researchers[8–14] for the control of the surface flow around the bluff bodies. The drag coefficient of a circular cylinder begins to decrease depending on the increasing turbulence intensity. The influence of a small rod on a downstream body is essentially similar of this effect. Hiwada et al.[8] investigated the fluid flow and heat transfer around two circular cylinders of different diameters in tandem. The upstream cylinder was used to act as a turbulence promoter to increase the heat transfer around the downstream one. Experimental work conducted by Igarashi[9] shows the existence of different flow patterns varying with spacing and Reynolds number for the smaller cylinder being downstream. Lesage and Gartshore[10] investigated the effect of a small circular cylinder on bluff bodies such as flat plates, square and circular cylinders. The authors reported the existence of a critical spacing where a sudden change in flow structure was detected. They also found that significant drag reduction was achieved in the case of a circular cylinder. Prasad and Williamson[11] studied the effects of a small flat plate at various locations of the main cylinder. An optimal geometrical configuration, which consisted of a plate height $\frac{1}{3}$ the cylinder diameter placed 1.5 diameter upstream of the cylinder and produced a system drag which was 38% that of the bare cylinder alone, was obtained. The reduction in drag appeared through two distinct modes of flow, a cavity mode for small values of plate-cylinder gap and a wake impingement mode for larger values of this gap. In the cavity mode, a larger drag reduction was observed because of a substantial increase in the thrust associated with the front surface of the cylinder.

Received 23 March 2004; revision received 28 June 2004; accepted for publication 9 January 2005.

*Assistant Professor, Department of Mechanical Engineering; sarioglu@ktu.edu.tr.

†Research Assistant, Department of Mechanical Engineering; currently Research Assistant, Department of Mechanical Engineering, Nigde University, 51200 Nigde, Turkey.

‡Professor and Head, Department of Mechanical Engineering.

Igarashi,[12] Tsutsui and Igarashi,[13] and Igarashi and Nobuaki[14] made a series of studies on drag reduction of bluff bodies such as a circular cylinder, a square cylinder, and flat plate. The bluff body was placed in the wake of a small rod to control the flow. For the square cylinder, two flow patterns with and without vortex shedding from the rod occurred according to the longitudinal spacing and rod diameter. The reduction of total pressure drag was 70% compared with that of the configuration without the rod.[12] For the circular cylinder, Tsutsui and Igarashi[13] investigated the flow pattern changes depending on the rod diameter, its position, and Reynolds number. The reduction of the total drag including the drag of the rod was 63% compared with that of a single cylinder. In the case of drag reduction of a flat plate normal to the airstream by flow control using a rod, the maximum reduction of total drag coefficient was about 20–30% compared to the values obtained without the rod in place.[14]

On the other hand, the occurrence of vortex shedding from a single square cylinder depends upon freestream flow characteristics and the angle of incidence to the flow. For a square cylinder at the angle of incidence in the range of $0 \text{ deg} \leq \theta \leq 45$ deg, large amounts of data concerning pressure distribution, vortex shedding, and drag coefficient have been provided by a number of authors.[15–23] These results essentially classified the flow around a square cylinder into two patterns less and beyond the angle at about 13 deg, where a sudden jump occurred in the Strouhal number. For angle $\theta < 13$ deg, the shear layer separated at the leading edge did not reattach on the lower side face of cylinder.[19] The other flow pattern, where reattachment of the separated shear layer was observed, took place beyond this angle. Chen and Liu[22] related the effect of the Reynolds number on the occurrence of such a jump in Strouhal number. For low Reynolds numbers ($Re = 2 \times 10^3$–3.3×10^3), the maximum Strouhal number was obtained at a relatively higher angle of 17 deg.

In the case of a square cylinder at an angle of incidence, the exact angle where reattachment begins to occur depends on the freestream turbulence.[15,18,22] For a square cylinder at zero angle of incidence placed in the wake of a small control rod, the boundary layer on both the side faces becomes turbulent for a spacing smaller than a critical gap. For larger values of this gap, vorticity is shed from the rod and the separated shear layers from the front edges of the square cylinder reattach on the side faces.[14] This is also important for a critical angle of incidence where the separated shear layer begins to reattach. Hence the present paper is aimed to investigate the influences of a small rod on the vortex shedding and the surface pressures of a square cylinder at incidence and to clarify the flow patterns and flow characteristics with respect to the angle of incidence and rod location.

II. Experimental Apparatus and Data Reduction

The experiments were conducted in the test section of a low-speed, open-type wind tunnel with a rectangular test section 289 mm wide, 457 mm high, and 1830 mm long. The two side Plexiglas® walls of the test section are tapered with a divergence angle of 0.3 deg on each side to provide a constant static pressure and to compensate for the boundary-layer growth along the tunnel axis. At the maximum tunnel speed of about 36 m/s, the freestream turbulence intensity was about 0.5%; the turbulence intensity was higher at low tunnel speeds, about 1.5% at 5 m/s, which is the lowest speed in the tunnel. The Reynolds number based on D, the width of the cylinder, was kept constant at 3.4×10^4 throughout the study, corresponding to a freestream velocity, 18 m/s, and a turbulence intensity of 0.8%. The tunnel and test section are shown in Fig. 1. A centrifugal fan draws air into a short constant pressure diffuser. This contains screens of comparatively high solidity, which have the effect of converting the highly nonuniform discharge from the fan to a much lower uniform axial velocity. The diffuser leads to a short settling length fitted with two further smoothing screens. This is followed by a contraction cone giving a contraction ratio of 10.9:1 and leading to the working section.

The test model consisted of two parts: the downstream square section cylinder and the upstream body shaped rod. The square cylinder was positioned at an angle of incidence to the freestream flow direction and turned in the range of $0 \text{ deg} \leq \theta \leq 45$ deg with

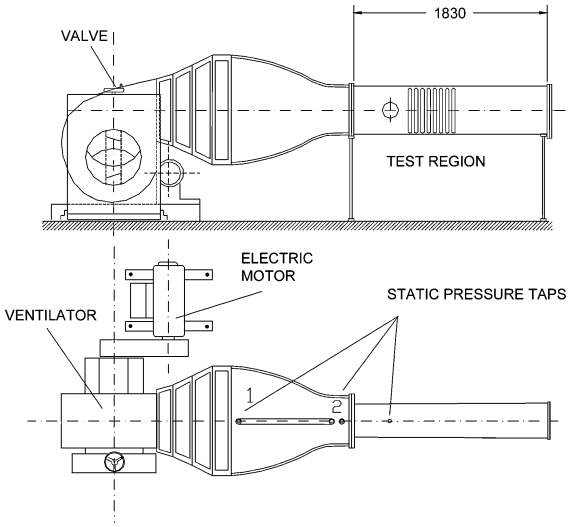

Fig. 1 Low-speed, open-type wind tunnel and test section.

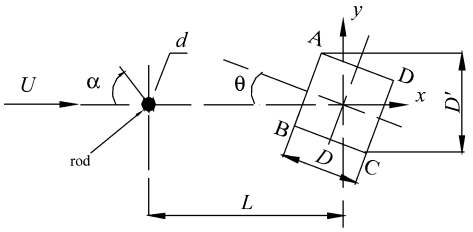

Fig. 2 Flow configuration and symbol definition.

an accuracy of ±0.5 deg. The square cylinder of 28 × 28 mm cross section spanned the entire width of the test section. A stainless-steel rod of 5 mm diam was used for the front body and the longitudinal distance between the axis of the square cylinder and rod was varied from 48 to 224 mm corresponding to $L/D = 1.71$–8.0. Both of the models were centered on the midheight of the test section with an accuracy of ±0.5 mm. The square cylinder model was constructed from Plexiglas and machined with sharp edges. The configuration of the present study is shown in Fig. 2. The solid blockage ratio of the square cylinder was changed from 6.1 to 8.6% as a result of the angle of incidence. By means of flow asymmetry caused by incidence, no correction was made for the blockage effects. As mentioned in Ref. 16, for a single square cylinder over the incidence range from 0 to 45 deg, resulting geometric blockages from 5.5 to 7.8%, the correction reduced the Strouhal number by an amount that varied between 4 and 5%. In the present study, as the rod in front of the square cylinder causes a smaller wake blockage than that of a square cylinder alone, the blockage effect can be expected to be smaller.

Vortex shedding from the square cylinder was detected by using a TSI IFA 100 model constant-temperature anemometer with a TSI 1210-20 hot-film probe. The Strouhal numbers for the vortex shedding from the models were determined from the frequency analysis of the velocity fluctuations. The probe was located in the center plane of the test section at approximately $6D$ downstream of the square cylinder and mounted on a traversing mechanism that could move it in the transverse direction in the range of $-2.5 < y/D < 2.5$.

Surface pressures were measured both on the square cylinder and rod. The coordinate system is shown in Fig. 2. The square cylinder had eight pressure taps 0.7 mm in diameter distributed at equal spacing on each surface, and there was only one pressure tap on the rod surface. The static pressure on the rod surface was measured at any angular position by turning the rod around its axis at desired circumferential angle α from the front stagnation point. Pressure measurements were made using a pressure transmitter in conjunction with the TSI Model 157 signal conditioner. The transmitter was connected to the pressure taps with Tygon tubes of 430-mm equal lengths and was referenced to the freestream wall pressure.

The hot-film probe was calibrated by using a TSI Model 1125 calibrator. The frequency response for the hot-film probe was found to be about 20 kHz by using a square-wave test. The velocity and pressure measurements were carried out using a computer-controlled data-acquisition system. For velocity measurements at each measurement point, 4096 data were acquired at a sampling rate of 1 kHz using a low-pass filter setting of 300 Hz. So the measuring time corresponded to 4.096 s. The pressure signals were acquired at a rate of 200 Hz and low-pass filtered at 100 Hz. Each of the mean pressures was obtained by means of integrating the time history of 8192 data for over 40 s. TSI Thermal-Pro Software was used to acquire signals with a 12-bit A/D converter and obtain the statistical results of these signals. The experimental uncertainty in the measurement of velocity was determined to be less than $\pm 3\%$, whereas that of pressure was determined to be less than $\pm 4\%$. The uncertainties in the drag coefficient, the Strouhal number, and the frequency spectra calculated from the experimental measurements were determined to be less than $\pm 4.8\%$ for the square cylinder ($\pm 4.2\%$ for the rod), ± 3.3, and $\pm 1\%$, respectively.

III. Experimental Results and Discussion

A. Mean Pressure Distribution

Measurements of surface pressure were carried out on the rod and square cylinder. First, the pressure distributions on the surfaces of the rod and square cylinder at zero angle of incidence were obtained to examine the effects caused by the change of flow patterns. Figure 3 shows the pressure distributions on the surface of the rod for $L/D = 1.71$–8.00 at the incidence angle of $\theta = 0$ deg.

The pressure distribution on the rod alone in a uniform flow is also presented in the same figure. As shown, there are two types of flow patterns: the pattern denoted by I or II was obtained for $L/D \geq 2.5$ and $L/D \leq 2.2$, respectively, as mentioned in the paper of Igarashi.[12] The flow pattern changes from II to I at about $L/D = 2.2$–2.5. There is a remarkable difference between patterns I and II on the rear side of the rod. In pattern I, the pressure distributions are very similar to a pressure distribution around a circular cylinder in a uniform subcritical flow and approximate the distribution on the rod alone with increased longitudinal spacing. In pattern II, it is seen in the figure that for $1.71 \leq L/D \leq 2.20$ the values of pressure coefficients on the rear side of the rod were at about zero, indicating a quasi-stationary vortex formation between the rod and the square cylinder.

The pressure distributions around the square cylinder with and without the rod are shown in Fig. 4 at the incidence angle of $\theta = 0$ deg. This figure shows that the pressures on the front surface of the square cylinder strongly depend on the location of the front rod. It is difficult to obtain the bilateral symmetry of pressure distribution at especially the front face, even if the rod were located in the center plane of flowfield of the square cylinder. This fact seen on the front face appeared in the studies of Igarashi[12] and Igarashi and Nobuaki,[14] where a square and a flat plate were used as a downstream body, respectively. This asymmetry has been associated with the interaction of the flow around the rod and the square cylinder and was very unstable.[14] In the figure, two flow regimes as also seen in Fig. 3 were observed so that the pressure distributions for $L/D = 1.71$–2.20 and $L/D \geq 2.50$ have different characteristics.

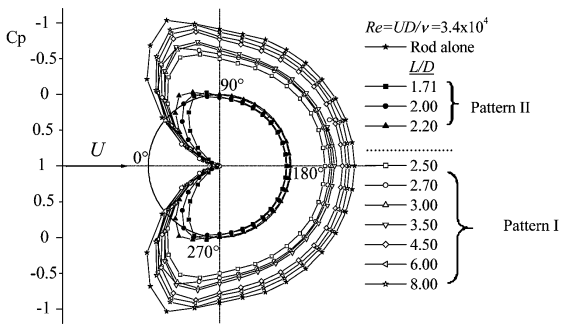

Fig. 3 Pressure distribution around the rod.

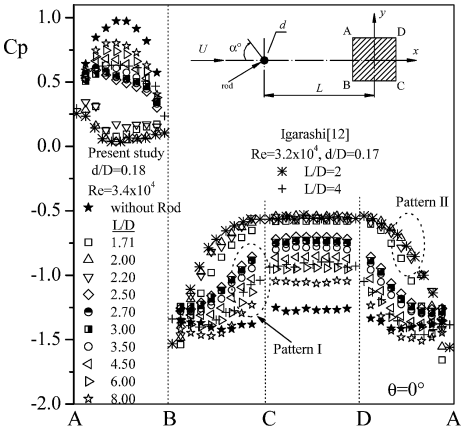

Fig. 4 Pressure distributions on the square cylinder with and without the rod at $\theta = 0$ deg.

For flow pattern II ($L/D < 2.5$), shear layers from the rod reattach on the front face of the square cylinder, and therefore the position of the maximum pressure moves from the centerline to the corners of the front face. At the beginning of pattern I, the pressure coefficient C_p has the value of 0.5 on the front face, smaller than the values without the rod, indicating a decrease of the approaching velocity to the square cylinder. As the spacing is increased up to $L/D = 8$, the pressure coefficients approach the values of the single square cylinder caused by the decreasing interaction of the two bodies. For the side and rear faces of the square cylinder, the effect of flow patterns on the pressure distributions is associated with a substantial change of the vortex formation region. In the case of pattern II, as the values of the pressure coefficient on the front face are lower than the values of pattern I, the pressures on the rear and side faces are higher.

These results agree to a great degree of the study conducted by Igarashi.[12] As a result of the pressure distributions around the rod and the square cylinder, there are two distinct modes of flow denoted as patterns I and II. Flow pattern I is associated with the occurrence of vortex shedding from the rod and the advancement of the distance required for vortex formation behind the square cylinder compared to that of the configuration without the rod.[12,14] Also, the shear layers separated from the front edges reattach on the side faces. For the flow pattern II, vortex shedding from the rod stops and the shear layers from the rod reattach on the front face. In this flow regime, the location of vortex formation of the square cylinder shifts downstream, indicating a rise of base pressure and a narrower wake width compared with that of pattern I.

In this study, the effects of incidence of the square cylinder with and without rod are examined. The well-known pressure distributions around a single square cylinder at incidence are shown in Fig. 5 and agree with the results in the study of Lee,[15] Igarashi,[21] Chen and Liu,[22] and Sarioglu and Yavuz.[23] This figure is given to show the effect of the rod on the angle of incidence. The pressure distributions on the front face vary with the rotation of the cylinder. On this face as θ increases, the position of maximum pressure moves from the centerline to the corner B. The upper side and the rear face are exposed to separated flow. The values of C_p on these faces increase gradually with increasing θ until the angle of sudden jump in Strouhal number occurs at $\theta = 13$ deg (as shown in Fig. 6), and then the values are lowered at $\theta \geq 15$ deg again. For the angle of incidence up to $\theta = 20$ deg, the base pressures are constant around -0.9 and -1.3, and then the pressure profiles on the both faces are symmetric with respect to the corner D. On the lower side face BC, a pressure recovery begins to appear at the jump angle about $\theta = 13$ deg, signifying possible reattachment of the shear layer as mentioned in the paper by Chen and Liu.[22] Accordingly, the drag coefficient on the square cylinder has a minimum value at the vicinity of the sudden jump angle (Fig. 7). When the cylinder is set at $\theta = 15$ deg, the pressure coefficient in the forward half of the face of BC drops to a minimum level, and the recovered pressure coefficients between the maximum and minimum values of C_p remain approximately

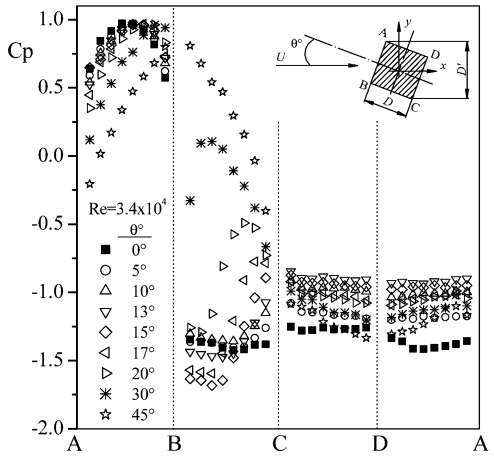

Fig. 5 Pressure distributions on the square cylinder without the rod.

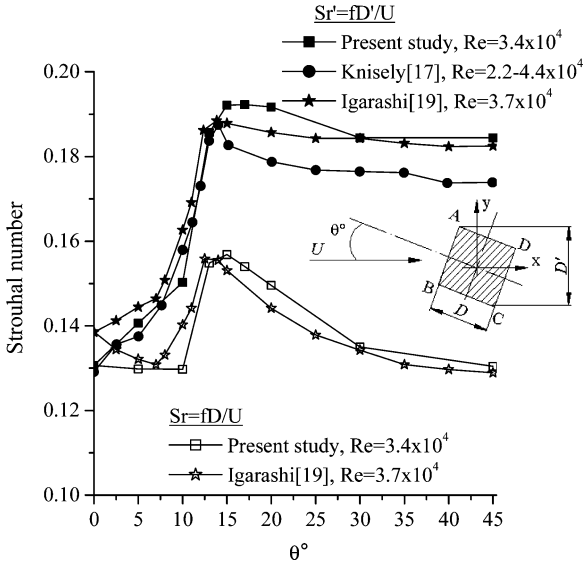

Fig. 6 Strouhal number vs the angle of incidence in the wake of the square cylinder without the rod.

the same until $\theta = 20$ deg. As the angle of incidence further increases from 20 to 30 deg, the maximum pressure coefficients on the side face BC rise considerably from -0.49 to 0.11, and this value reaches 0.81 at 45 deg. As expected, at the angle of $\theta = 45$ deg there is a symmetry between the pressures on the faces AB and BC and CD and DA.

The major purpose of this study as just mentioned is to investigate the effect of the rod on the square cylinder in incidence. The variations of pressure coefficients on the square cylinder in incidence with the rod are shown in Figs. 8–11 for $L/D = 1.71$, 2.70, 3.50, and 6.00. There are considerable differences in the pressure profiles on the faces AB and BC between $L/D = 1.71$ and $L/D \geq 2.7$. The pressures on these surfaces for $L/D \geq 2.7$ are relatively similar to those on these surfaces for the square cylinder without the rod (Fig. 5). There are important changes in the flow around the cylinders for $L/D = 1.71$ because of the interaction of the flow around the rod and square cylinder.

As shown in Fig. 8, at 0-deg incidence the shear layers separated from the lower and upper side of the rod reattach on the edges of the front face (AB). When the square cylinder is set at the nonzero angle of incidence, the shear layer separated from upper side of the rod reattaches on the face AB and then proceeds to both corners A and B. Meanwhile, quasi-stationary vortices belonging to pattern II occur between the rod and cylinder. However, the shear layer separated from lower side of the rod does not reattach on the face AB. This point was also verified by smoke-visualization results shown

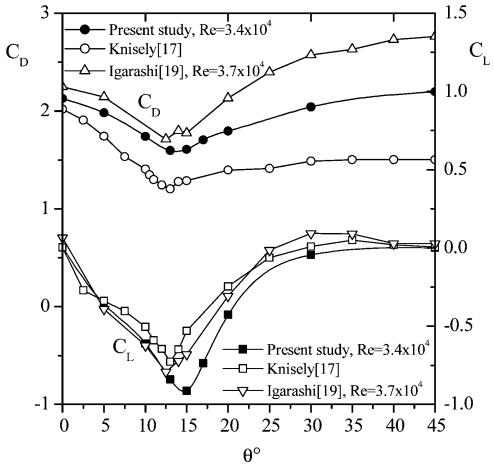

Fig. 7 Drag and lift coefficients on the square cylinder without the rod in incidence.

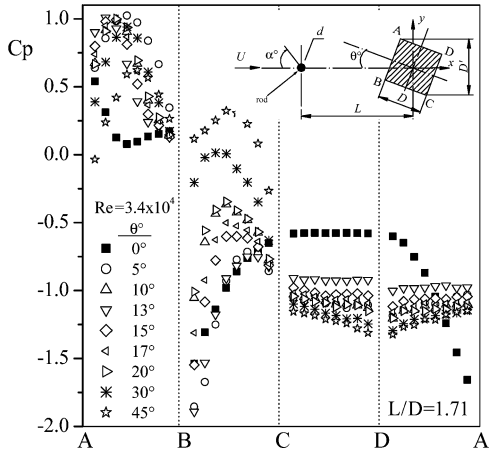

Fig. 8 Pressure distributions on the square cylinder for *L/D* = 1.71.

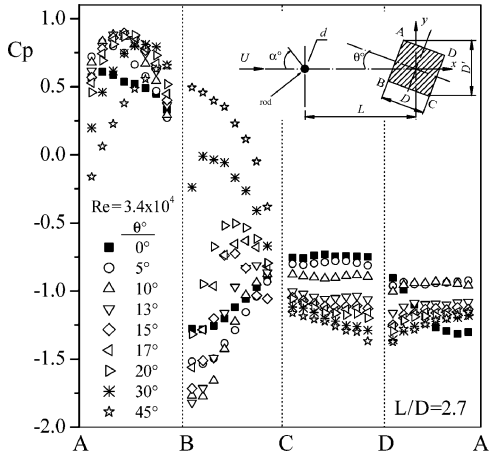

Fig. 9 Pressure distributions on the square cylinder for *L/D* = 2.7.

in Figs. 12 and 13. There is no reattachment on the side faces at 0-deg incidence, as confirmed by Igarashi.[12] However, at nonzero incidence there are reattachments on face B: shear layers from the corner B reattach on this surface up to $\theta = 17$ deg, and then the shear layers from the rod reattach. As a weak reattachment occurs near the corner C at $\theta = 5$ and 13 deg, their pressure levels are the same. At $\theta = 10$ deg, the reattachment occurs at near the center of the surface and results in a strong pressure recovery. The shear layer separated from the lower side of the rod becomes parallel to the face BC, and the pressure level on this face reduces because of increasing

velocity in this region. The point of maximum pressure coefficient, at the center of face BC at $\theta = 15$ deg, moves to the corner B up to $\theta = 30$ deg. In this range of θ, the pressure recovery gradually appears on this surface. At $\theta = 45$ deg, the reattachment of the shear layer from the rod occurs at the center of both faces AB and BC, whereas the attachment is at the stagnation point, the corner B, in the case of without rod (Fig. 5). Therefore, the pressure coefficients reach positive values at this angle of incidence. The pressures on the face CD for $L/D = 1.71$ decrease as θ increases from 0 to 5 deg and then with a further increase in θ they increase first until 13 deg and then decrease after 13 deg. Conversely, the pressures on this surface decrease gradually with increasing θ for $L/D = 2.7$ and 3.5.

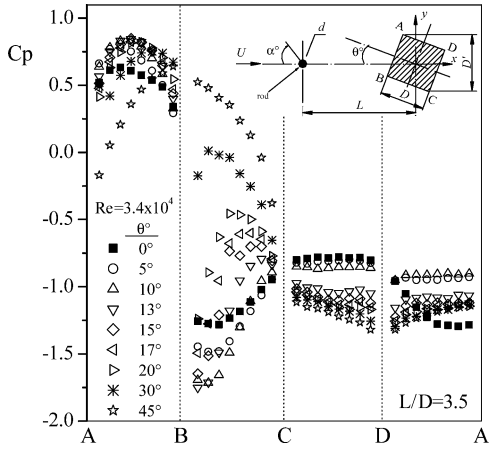

Fig. 10 Pressure distributions on the square cylinder for *L/D* = 3.5.

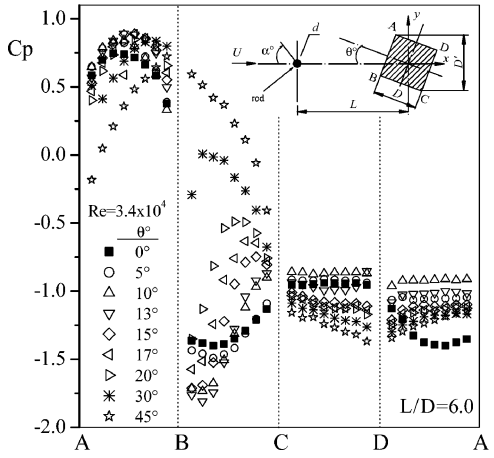

Fig. 11 Pressure distributions on the square cylinder for *L/D* = 6.0.

As shown in Figs. 9–11, it can be said that flow pattern I is observed in the cases of $L/D \geq 2.5$ at all angles of incidence considered. This is also observed in the smoke-visualization tests presented in Fig. 13. For $L/D \geq 2.5$, the pressure profiles on AB and BC seem relatively same to those for the square cylinder without the rod because of reduced rod effects, where the flow behind the rod becomes an approaching flow to the square cylinder. The pressure distribution on the lower side face BC varies with increasing angle of incidence: shear layers separated from corner B reattach on the face BC, and the position of reattachment shifts from the corner C to the corner B at $\theta \leq 20$ deg. As θ is increased to 30 and 45 deg, attachments (not reattachments) of approaching flow from the rod occur near the corner B. The pressure on the rear face DC reduces to a minimum level.

B. Flow Visualization

The effects of the rod on the square cylinder at incidence can be seen in Figs. 12a and 12b obtained from flow-visualization tests in a small smoke tunnel.

The blockage ratio and the ratio of upstream body scale to downstream body scale d/D for the smoke tunnel flow visualizations were about the same as that of the wind-tunnel tests. The Reynolds number was about 3.5×10^3 based on the square cylinder diameter and the velocity in the smoke tunnel. Although this Reynolds number was smaller than that of the primary tests in the wind tunnel, it was seen that the types of flow patterns visualized in both of the cases of $L/D = 1.71$ and 3.5 in the smoke tunnel agreed well with the patterns obtained in the wind tunnel. Because of the sharp edges, the flow pattern is not changed with the Reynolds number. This point is also mentioned by Igarashi and Nobuaki[14] that the drag coefficient and the Strouhal number are independent of the Reynolds number in the same pattern. Therefore, the flow visualizations conducted with $Re = 3.5 \times 10^3$ can be adopted to simulate the corresponding flow behavior measured in the wind tunnel. In Fig. 12a for $L/D = 1.71$, quasi-stationary vortices are formed between the rod and cylinder at all angles of incidence, where the flow pattern is II without vortex shedding from the rod. These vortices are also seen in the photographs of flow visualization conducted by Igarashi.[12] In Fig. 12b for $L/D = 3.5$, vortex shedding from the rod is observed in the gap, denoted as pattern I. It is seen that in both the patterns I and II the widths of the wake behind the square cylinder increase as the angle of incidence increases. Flow visualization was also performed using the smoke-wire method in the wind tunnel with the same model for $Re = 7.5 \times 10^3$ (Fig. 13).

In Fig. 13a, for the square cylinder alone and rod-square cylinder bodies for $L/D = 1.71$ and 3.5 flow-visualization photographs are shown for $\theta = 0$ deg. In Fig. 13b, at various angles of incidence

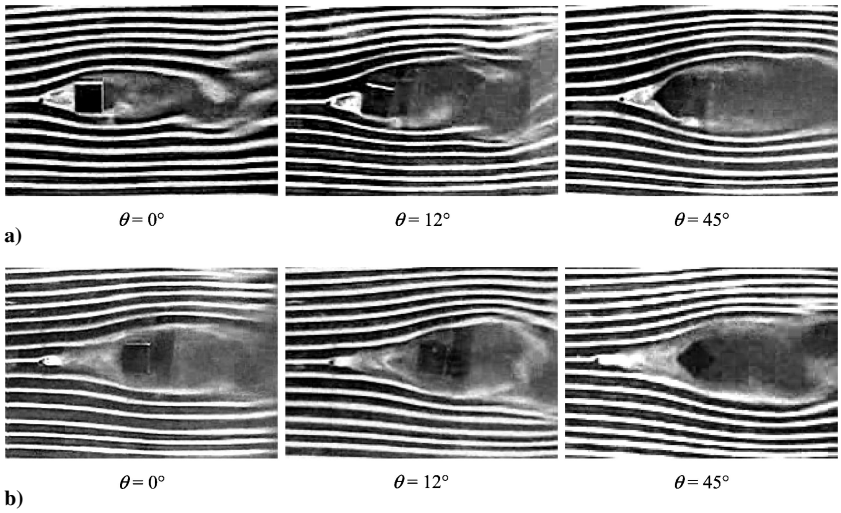

Fig. 12 Flow visualization using by smoke tunnel for a) *L/D* = 1.71 and b) *L/D* = 3.5.

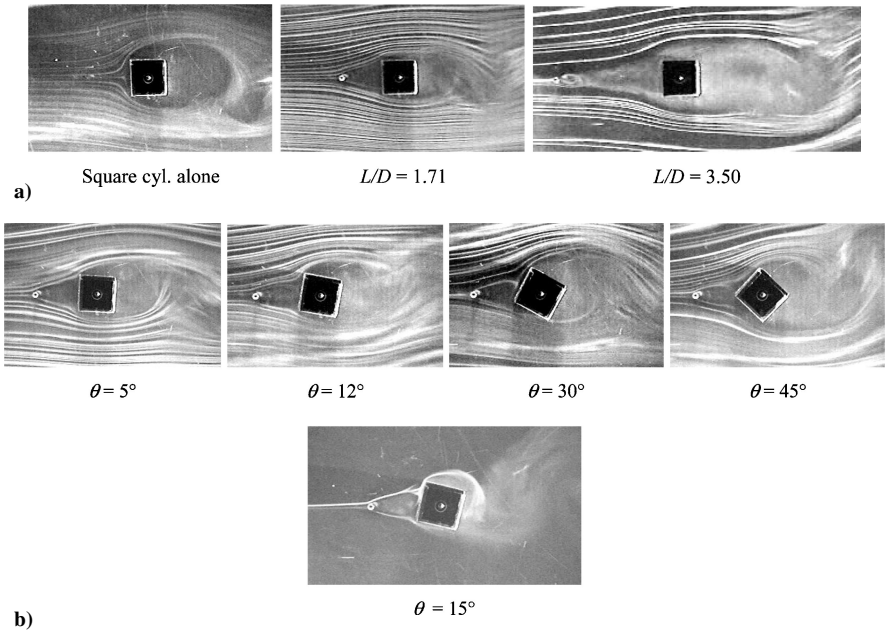

Fig. 13 Smoke-wire visualization of the flow around rod-square cylinder bodies for $Re = 7.5 \times 10^3$: a) $\theta = 0$ deg and b) $L/D = 1.71$.

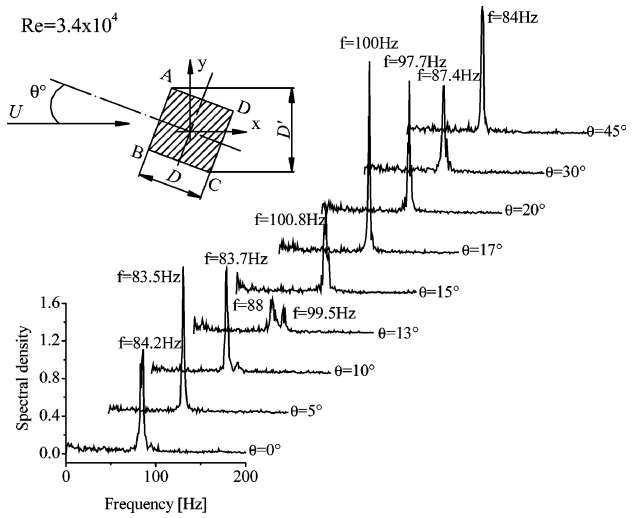

Fig. 14 Spectra in the wake of the square cylinder without the rod for different incidences.

flow-visualization photographs are given for $L/D = 1.71$. As shown in these photographs, because of the higher Reynolds number and aspect ratio, quasi-stationary vortices cannot be observed clearly, unlike the cases shown in Fig. 12a.

C. Vortex-Shedding and Strouhal Number

The vortex-shedding phenomenon is very important in the flow around bluff bodies. The vortex shedding from the square cylinder was examined at the Reynolds number of 3.4×10^4. The velocity signal was measured in the wake of the square cylinder at $x/D = 6$ and $y/D = 1.0$, where x/D and y/D are the downstream and vertical distances, respectively. Plots of the velocity spectra at $\theta =$ 0–45 deg in the wake of the square cylinder without the rod are given in Fig. 14, where the spectral density is plotted against frequency. As shown in this figure, it is observed that single peaks occur at all angles of incidence considered except for 13 deg. At 13-deg incidence, two peaks are observed and associated with the reattachment of the separated shear layer on the lower side surface of the square cylinder.

The Strouhal numbers $Sr' = f \cdot D'/U$, where D' is the projected cross-stream dimension of the square cylinder, vs the angle of incidence θ obtained in the wake of the square cylinder without the rod are given in Fig. 6.

As shown in the figure, the Strouhal number increases gradually with increasing angle of incidence and has a jump at 13 deg. Thereafter, it reaches a maximum at about 15 deg. Then it decreases slightly as expected. Examining the Strouhal-number values, it is seen that the results are in good agreement with those obtained by Igarashi[19] at similar experimental conditions ($Re = 3.7 \times 10^4$, turbulence intensity = 0.5%, and $D = 29.2$ mm).

In the case of the square cylinder with the rod, the Strouhal number vs angle of incidence obtained for different values of L/D are presented in Fig. 15. The influences of both L/D and θ on Strouhal number can be seen in Fig. 16. In this figure, at small angles of incidence the influence of the flow type on the Strouhal number is important, and there is a drastic decrease in Strouhal number. For $\theta < 13$ deg, this is explained by the reattachments on the front face AB in pattern II. From $\theta = 13$ deg, this effect of the flow decreases, and the effect of the angle of incidence on Strouhal number becomes dominant. When these results in this figure are compared with the values of Igarashi[12] (for the case of $\theta = 0$ deg and $d/D = 0.17$), it is seen that the sudden change from pattern I to pattern II in flow structure occurs at the same value of L/D.

D. Drag and Lift Coefficients

The drag and lift coefficients, based on D as the reference length, of the square cylinder were obtained by the integration of the pressure distributions with Eqs. (1) and (2) and shown in Figs. 7 and 17–19:

$$C_D = \left(\int_A^B C_p \cdot \cos\theta \cdot \mathrm{d}s + \int_B^C C_p \cdot \sin\theta \cdot \mathrm{d}s - \int_C^D C_p \cdot \cos\theta \cdot \mathrm{d}s - \int_D^A C_p \cdot \sin\theta \cdot \mathrm{d}s \right) \Big/ D \tag{1}$$

$$C_L = \left(-\int_A^B C_p \cdot \sin\theta \cdot \mathrm{d}s + \int_B^C C_p \cdot \cos\theta \cdot \mathrm{d}s + \int_C^D C_p \cdot \sin\theta \cdot \mathrm{d}s - \int_D^A C_p \cdot \cos\theta \cdot \mathrm{d}s \right) \Big/ D \tag{2}$$

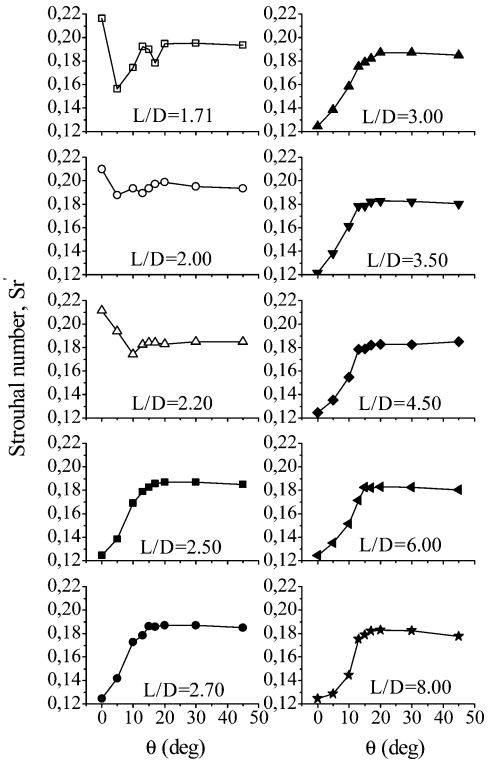

Fig. 15 Strouhal number vs angle of incidence in the wake of the square cylinder for different values of *L/D*.

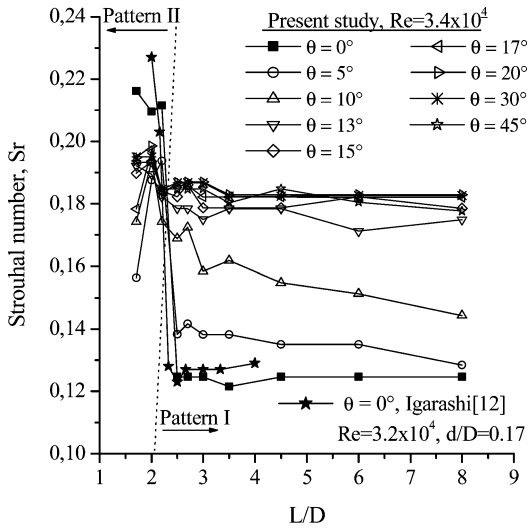

Fig. 16 Strouhal number vs *L/D* in the wake of the square cylinder for a different angle of incidence.

Figure 7 shows the variation of C_D and C_L of the square cylinder vs the incidence without rod. The drag coefficient decreases from a high initial value to a minimum in the region 13–15 deg, corresponding to a sudden jump in the Strouhal number, and subsequently increases steadily until $\theta = 45$ deg. Minimum values of C_L and C_D at this angle are associated with the reattachment of the shear layer to the lower side face. Figure 7 also includes the data of Igarashi[19] and Knisely,[17] and the present data of C_D agree with their results.

There is a change in the drag coefficient with the existence of the rod because the rod changes the effective upstream shape of the square cylinder. The total drag coefficients including the rod C_{DT} are given as $C_{DT} = C_D + C_{DR} \cdot (d/D)$ presented in Ref. 12. This additional drag caused by the rod is added proportionally with the

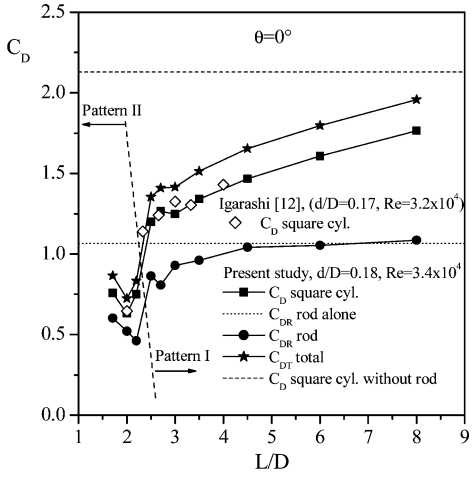

Fig. 17 Drag coefficient on the rod and square cylinder vs *L/D* at $\theta = 0$ deg.

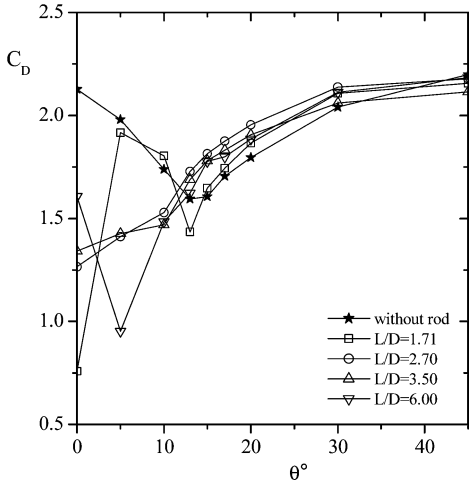

Fig. 18 Drag coefficients on the square cylinder with and without the rod.

ratio of the diameters of the bodies. Figure 17 shows the drag coefficients of both the square cylinder and rod C_D and C_{DR} and also total drag coefficient C_{DT} at $\theta = 0$ deg. As shown in this figure, the drag coefficient in pattern II is smaller to that in pattern I, corresponding to a sharp decrease in vortex shedding frequency (Fig. 16). In the range of $L/D = 1.71$–8.0, as drag coefficient of the rod changes from the minimum value of 0.46 to 0.86, with a further increase in L/D it reaches the value corresponding to the rod alone. The minimum value of drag coefficient on the square cylinder is obtained for $L/D = 2.0$ and produces a drag that is 30% that of the square cylinder without rod. The results of Igarashi[12] for a similar case are also shown in Fig. 17, and there is a good agreement between the drag coefficient values.

Figures 18 and 19 show the variation of drag and lift coefficients on the square cylinder with the angle of incidence for $L/D = 1.71$, 2.70, 3.0, and 6.0.

As shown in these figures, at small angles of incidence it is evident that the significant effect of interference occurs for the small spacing, that is, $L/D = 1.71$, and this can be associated with pattern II. For larger angles, $\theta \geq 15$ deg, the effect of L/D is weaker than that of the angle of incidence, and the variation of the drag coefficients is similar to that of the square cylinder without rod (Fig. 7). Except for $L/D = 1.71$, the variation of the lift coefficient has a similar character to that of the square cylinder without rod, and the minimum value occurs at $\theta = 10$ deg for $L/D = 2.7$ and 3.5, and with further increasing L/D this value gradually approaches that of the square cylinder without the rod.

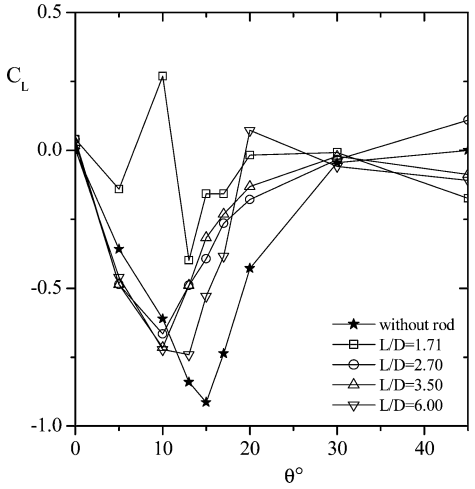

Fig. 19 Lift coefficients on the square cylinder with and without the rod.

IV. Conclusions

To investigate the effects of a rod on the flow around a square cylinder at incidence, a rod was set upstream of the square cylinder. The diameter of the rod was 5 mm, the length of side of the square cylinder was 28 mm, and the corresponding Reynolds number was $Re = 3.4 \times 10^4$. The following conclusions were obtained:

According the spacing L/D, two flow patterns with and without vortex shedding from the rod were obtained: patterns II and I for $L/D \leq 2.2$ and ≥ 2.5, respectively.

Pressure distributions on the square cylinder were obtained as a function of L/D and angle of incidence θ. For $L/D = 1.71$ (pattern II), there is no reattachment on the side faces at 0-deg incidence. However, at nonzero incidence reattachments occur on the face BC: shear layers from the corner B reattach on this surface up to $\theta = 17$ deg, and then shear layers from the rod reattach. Reattachments occur on the side faces after $\theta = 13$ deg. For $L/D \geq 2.50$ (pattern I), the pressure distribution on the lower side face BC varies with increasing angle of incidence: shear layers separated from corner B reattach on BC surface, and the position of the reattachment point shifts from the corner C to corner B at $\theta \leq 20$ deg. As θ is increased to 30 and 45 deg, attachments (not reattachments) of approaching flow from the rod occur near corner B.

For $L/D \leq 2.20$ (pattern II), the Strouhal number of the square cylinder initially decreases with the angle of incidence and reaches a minimum value. Then the Strouhal number increases to an approximately constant value at a certain angle of θ. For $L/D \geq 2.50$ (pattern I), the variation of Strouhal number with the angle of incidence is relatively similar to that of the square cylinder without rod. That is, the Strouhal number increases with the angle of incidence and reaches a constant value at about 17 deg.

At zero angle of incidence, the minimum value of drag on the square cylinder is obtained for $L/D = 2.0$ and produces a drag that is 30% that of the square cylinder without the rod. For $L/D = 1.71$ at 0-deg incidence, as the value of C_D of the square cylinder reduces to 36% of that of the square cylinder without rod, with increasing the angle of incidence these C_D values approximate to those of the square cylinder without rod. For $L/D \geq 2.5$, there is a considerable decrease in C_D for $\theta \leq 10$ deg; however, the effect of the rod on C_D decreases beyond $\theta = 10$ deg.

References

[1]Shiraishi, N., Matsumoto, M., and Shirato, H., "On Aerodynamic Instabilities of Tandem Structures," *Journal of Wind Engineering and Industrial Aerodynamics*, Vol. 23, No. 1–3, 1986, pp. 437–447.

[2]Zdravkovich, M. M., and Pridden, D. L., "Interference Between Two Circular Cylinders: Series of Unexpected Discontinuities," *Journal of Industrial Aerodynamics*, Vol. 2, No. 3, 1977, pp. 255–270.

[3]Arie, M., Kiya, M., Moriya, M., and Mori, H., "Pressure Fluctuating on the Surface of Two Circular Cylinders in Tandem Arrangement," *Journal of Fluids Engineering*, Vol. 105, 1983, pp. 161–167.

[4]Okajima, A., "Flows Around Two Tandem Circular Cylinders at Very High Reynolds Numbers," *Bulletin of the JSME*, Vol. 22, No. 166, 1979, pp. 504–511.

[5]Igarashi, T., "Characteristic of the Flow Around Two Circular Cylinders Arranged in Tandem," *Bulletin of the JSME*, Vol. 24, No. 188, 1981, pp. 323–331.

[6]Gu, Z., "On Interference Between Two Circular Cylinders at Supercritical Reynolds Numbers," *Journal of Wind Engineering and Industrial Aerodynamics*, Vol. 62, May 1996, pp. 175–190.

[7]Alam, Md. M., Moriya, M., Takai, K., and Sakamoto, H., "Fluctuating Fluid Forces Acting on two Circular Cylinders in a Tandem Arrangement at a Subcritical Reynolds Number," *Journal of Wind Engineering and Industrial Aerodynamics*, Vol. 91, No. 1–2, 2003, pp. 139–154.

[8]Hiwada, M., Taguchi, T., Mabuchi, I., and Kumada, M., "Fluid Flow and Heat Transfer Around Two Circular Cylinders of Different Diameters in Cross Flow," *Bulletin of the JSME*, Vol. 22, No. 167, 1979, pp. 715–723.

[9]Igarashi, T., "Characteristic of a Flow Around Two Circular Cylinders of Different Diameters Arranged in Tandem," *Bulletin of the JSME*, Vol. 25, No. 201, 1982, pp. 349–357.

[10]Lesage, F., and Gartshore, I. S., "A Method of Reducing Drag and Fluctuating Side Force on Bluff Bodies," *Journal of Wind Engineering and Industrial Aerodynamics*, Vol. 25, No. 2, 1987, pp. 229–245.

[11]Prasad, A., and Williamson, C. H. K., "A Method for the Reduction of Bluff Body Drag," *Journal of Wind Engineering and Industrial Aerodynamics*, Vol. 69–71, July–Oct. 1997, pp. 155–167.

[12]Igarashi, T., "Drag Reduction of a Square Prism by Flow Control Using a Small Rod," *Journal of Wind Engineering and Industrial Aerodynamics*, Vol. 69–71, 1997, pp. 141–153.

[13]Tsutsui, T., and Igarashi, T., "Drag Reduction of a Circular Cylinder in an Air-Stream," *Journal of Wind Engineering and Industrial Aerodynamics*, Vol. 90, No. 4–5, 2002, pp. 527–541.

[14]Igarashi, T., and Nobuaki, T., "Drag Reduction of Flat Plate Normal to Airstream by Flow Control Using a Rod," *Journal of Wind Engineering and Industrial Aerodynamics*, Vol. 90, No. 4–5, 2002, pp. 359–376.

[15]Lee, B. E., "The Effect of Turbulence on the Surface Pressure Field of a Square Prism," *Journal of Fluid Mechanics*, Vol. 69, Part 2, 1975, pp. 263–282.

[16]Obasaju, E. D., "An Investigation of the Effects of Incidence on the Flow Around a Square Section Cylinder," *Aeronautical Quarterly*, Vol. 34, Nov. 1983, pp. 243–259.

[17]Knisely, C. W., "Strouhal Numbers of Rectangular Cylinders at Incidence: A Review and New Data," *Journal of Fluids and Structures*, Vol. 4, No. 4, 1990, pp. 371–393.

[18]Vickery, B. J., "Fluctuating Lift and Drag on a Long Cylinder of a Square Cross-Section in a Smooth and in a Turbulent Stream," *Journal of Fluid Mechanics*, Vol. 25, Part 3, 1966, pp. 481–494.

[19]Igarashi, T., "Characteristics of the Flow Around a Square Prism," *Bulletin of the JSME*, Vol. 27, No. 231, 1984, pp. 1858–1865.

[20]Igarashi, T., "Heat Transfer from a Square Prism to an Air Stream," *International Journal of Heat and Mass Transfer*, Vol. 28, No. 1, 1985, pp. 175–181.

[21]Igarashi, T., "Local Heat Transfer from a Square Prism to an Airstream," *International Journal of Heat and Mass Transfer*, Vol. 29, No. 5, 1986, pp. 777–784.

[22]Chen, J. M., and Liu, C. H., "Vortex Shedding and Surface Pressures on a Square Cylinder at Incidence to a Uniform Air Stream," *International Journal of Heat and Fluid Flow*, Vol. 20, No. 6, 1999, pp. 592–597.

[23]Sarioglu, M., and Yavuz, T., "Subcritical Flow Around Bluff Bodies," *AIAA Journal*, Vol. 40, No. 7, 2002, pp. 1257–1268.

J. Gore
Associate Editor